



## LJMU Research Online

**Yu, Z, Connolly, DP, Woodward, PK, Laghrouche, O and Tutumluer, E**

**Railway ballast anisotropy testing via true triaxial apparatus**

<http://researchonline.ljmu.ac.uk/id/eprint/16611/>

### Article

**Citation** (please note it is advisable to refer to the publisher's version if you intend to cite from this work)

**Yu, Z, Connolly, DP, Woodward, PK, Laghrouche, O and Tutumluer, E (2020) Railway ballast anisotropy testing via true triaxial apparatus. *Transportation Geotechnics*, 23. ISSN 2214-3912**

LJMU has developed **LJMU Research Online** for users to access the research output of the University more effectively. Copyright © and Moral Rights for the papers on this site are retained by the individual authors and/or other copyright owners. Users may download and/or print one copy of any article(s) in LJMU Research Online to facilitate their private study or for non-commercial research. You may not engage in further distribution of the material or use it for any profit-making activities or any commercial gain.

The version presented here may differ from the published version or from the version of the record. Please see the repository URL above for details on accessing the published version and note that access may require a subscription.

For more information please contact [researchonline@ljmu.ac.uk](mailto:researchonline@ljmu.ac.uk)

<http://researchonline.ljmu.ac.uk/>

# Railway ballast anisotropy testing via true triaxial apparatus

Zelong Yu<sup>1,2,\*</sup>, D. P. Connolly<sup>3</sup>, P. K. Woodward<sup>3</sup>, O. Laghrouche<sup>2</sup>, E. Tutumluer<sup>4</sup>,

<sup>1</sup> Newcastle University, School of Civil Engineering & Geosciences, Newcastle Upon Tyne, NE1 7RU, UK  
E-mail: [Zelong.Yu@newcastle.ac.uk](mailto:Zelong.Yu@newcastle.ac.uk)

<sup>2</sup> Heriot-Watt University, Institute for Infrastructure and Environment, Edinburgh, EH14 4AS, UK  
E-mail: [O.Laghrouche@hw.ac.uk](mailto:O.Laghrouche@hw.ac.uk)

<sup>3</sup> University of Leeds, Institute for High Speed Rail and Systems Integration. Leeds, LS2 9JT, UK  
E-mail: [d.connolly@leeds.ac.uk](mailto:d.connolly@leeds.ac.uk); [P.K.Woodward@leeds.ac.uk](mailto:P.K.Woodward@leeds.ac.uk)

<sup>4</sup> University of Illinois at Urbana-Champaign, Department of Civil and Environmental Engineering, 205 N. Mathews, Urbana, IL 61801, United States  
E-mail: [tutumlue@illinois.edu](mailto:tutumlue@illinois.edu)

\* Corresponding author

## Abstract

This paper aims to demonstrate the anisotropic behaviour of railway ballast via true-triaxial tests. To do so, a novel, large-scale, true-triaxial testing apparatus (GeoTT) is designed and constructed. It consists of six hydraulic actuators, designed to apply a distributed stress to large granular cubic test specimens with dimensions: 500mm × 500mm × 500mm. To show the capability of the new facility, crushed granite railway ballast with  $d_{50}=43\text{mm}$  is tested. Three different confining stresses are applied to determine the Poisson's ratio and modulus in three dimensions. Anisotropic behaviour is clearly evident, with horizontal directions showing a lower modulus compared to the vertical direction. It is also found that confining stress has an important effect on both Poisson's ratio and modulus when the primary loading is applied in three orthogonal directions. These results are useful for understanding the behaviour of railway ballast and for the calibration of railroad numerical models.

**Key words:** Granular particle anisotropy; Railway ballast; true triaxial testing (GeoTT), Ballast modulus; Poisson's ratio; Railroad

## 1 Introduction

Granular soils are often referred to as aggregates and are a common construction material for pavements and railways. A large number of studies have been undertaken to quantify the isotropic behaviour of granular particles, including [1–8]. Testing of granular materials with large maximum particle size requires a larger-scale testing apparatus compared to the testing of smaller particles. This is because larger sample volumes are required to ensure the ratio between maximum particle size and sample dimension is low.

Although isotropic loading tests provide insights into material behaviour, many granular materials actually behave in an anisotropic manner [9–12]. Table 1 outlines a range of studies performed using traditional triaxial cells to explore the anisotropy of response. The anisotropic behaviour of ballast is of significance for railway tracks

42 because it aids the understanding of ballast behaviour in the horizontal direction.  
43 This is particularly important for tracks in curves. Further, it is an important material  
44 input when numerically modelling ballast.

45 However, investigating anisotropy ideally requires the test sample to be  
46 subject to a range of stress paths that are difficult to achieve using standard triaxial  
47 testing. Therefore, the two most common approaches to achieve this are: Hollow  
48 Cylinder Apparatus (HCA) and true triaxial (TT) testing. HCA methods are useful for  
49 simulating the rotation of principal stresses that occur during wheel passage.  
50 Alternatively, TT methods account for the effect of intermediate principal stresses,  
51 which in reality, may be different from the minor principal stresses when considering  
52 full anisotropy.

53 HCA works by subjecting a hollow, cylindrical soil sample to an axial load and  
54 torque about the central vertical axis, while applying external and internal radial  
55 pressures. The torque results in shear stress while the axial load combined with the  
56 radial pressures results in vertical stress [13–16].

57 The majority of HCA research into granular particle anisotropy to-date has  
58 focused on materials with relatively small maximum particle size (see Table 2). For  
59 example, Tatsuoka et al. [17], Pradhan et al. [18] and Pradhan et al. [19] tested soil  
60 specimens with an inner diameter, outer diameter and height of 60mm, 100mm and  
61 200mm, respectively. They investigated the strength and deformation properties of  
62 Toyoura sand. Alternatively, Yang et al. [20] used larger HCA apparatus to investigate  
63 the anisotropic behaviour of saturated sand. Alternatively, Lade et al. [21] and Lade  
64 [22] used HCA tests to study the cross-anisotropic behaviour of Santa Monica beach  
65 sand and found that cross-anisotropy correlated with increasing inclinations of the  
66 major principal stress direction. O’Kelly and Naughton [23], O’Kelly and Naughton  
67 [24], Yang [25], Yang et al. [26] and Rolo [27] also used HCA testing to investigate the  
68 anisotropic behaviour of sands.

69 As an alternative to HCA testing, TT testing works by subjecting a soil sample  
70 to stresses in the three orthogonal planes, often using two hydraulic actuators in each  
71 plane, either via rigid flat plates or flexible membranes or a mixture of both (see Table  
72 3 for a summary of previous studies). Sture and Desai [28] and Desai et al. [29]  
73 developed true triaxial test setups to apply a three-dimensional, independently  
74 controlled, and compressive stress state, using fluid or pneumatically pressurized  
75 flexible cushions to transmit stresses in three orthogonal directions, to a cubic sand-  
76 ballast specimen with dimensions 101.6mm × 101.6mm × 101.6mm. Isotropic loading  
77 was applied to specimens to determine anisotropic response behaviour (i.e.,  
78 directional dependencies of compacted specimen responses). Alternatively, Yamada  
79 and Ishihara [30] used true triaxial apparatus with a cubic sand specimen of  
80 dimensions 100mm × 100mm × 100mm. Results indicated that behaviour was highly  
81 anisotropic, inherently due to grain orientation, size and shape. However, as the  
82 applied shear stress increased, at failure, the inherent anisotropic effects  
83 disappeared.

84 Alternatively, Reis et al. [31] developed a cubic triaxial cell to test 60mm  
 85 specimens of saturated and unsaturated soil. Further, Ochiai and Lade [32] used true  
 86 triaxial apparatus to study the anisotropic behaviour of Cambria sand and found that  
 87 the major principal strain was the lowest when the dilation rate was at a maximum.  
 88 The same apparatus was then used to develop a failure criterion for cross-anisotropic  
 89 soils [33,34].

90 Furthermore, Tutumluer and Seyhan [35] and Seyhan and Tutumluer [36] used  
 91 a triaxial device to test aggregate samples with 150 mm diameter and 150 mm height.  
 92 The vertical modulus was found to be larger than the horizontal modulus for all tested  
 93 aggregates except one gravel specimen which contained 16% fines (defined as passing  
 94 the No. 200 sieve or smaller than 0.075 mm) in a dense-graded base course aggregate  
 95 with a maximum size of 25 mm.

96 When testing granular particles, it is important to maximise the sample size-  
 97 to-particle ratio, defined as the minimum dimension of the test sample divided by  
 98 maximum particle size. If too small, individual particles dominate test results thus  
 99 causing testing errors. As a guide, Nitchiporovitch [37] and Fagnoul and Bonnechere  
 100 [38] suggested a minimum sample size-to-particle ratio of 5, while Marachi et al. [39]  
 101 proposed a ratio of 6. Therefore, because the width of the HCA wall is relatively thin,  
 102 it is not well-suited for testing large diameter particles. True triaxial apparatus is  
 103 arguably better suited because it can house a cuboidal volume of granular material,  
 104 with potentially larger dimensions than the HCA. However, even then, it is  
 105 challenging to construct a TT apparatus of sufficient scale to investigate the  
 106 anisotropy of samples containing large granular particles.

107 This paper addresses these sample size challenges by developing a new TT facility  
 108 capable of testing soil samples with dimensions: 500mm x 500mm x 500mm. The  
 109 large potential test volume means it is well suited to testing large-particle granular  
 110 soils, including railway ballast. The maximum particle size tested in this study was  
 111 63mm, giving a sample size-to-particle ratio of approximately 8. The facility was used  
 112 to apply tri-directional stress patterns to railroad ballast and investigate its  
 113 anisotropic behaviour. Considering that previous research has focused on the  
 114 relationship between confining stress and Poisson's ratio in the vertical direction only,  
 115 this paper extends this concept to the relationship in the horizontal direction.

116

117 Table 1. Anisotropic tests conducted using traditional triaxial cells

Source	Soil type	Dimension (mm)	Aim
Miura et al. [9]	Sand	Diameter =70mm, Height = 170mm	Anisotropy, stress- strain curves, liquefaction
Tutumluer and Seyhan [35] and Seyhan and Tutumluer [36]	Aggregate	Diameter =150mm Height =150mm	Anisotropy, resilient behaviour

Rolo [27]	Sand/clay	Diameter =100mm Height =200mm	Anisotropy, shear strength
Aursudkij et al. [40]	Ballast	Diameter =150mm Height =450mm	Resilient modulus and Poisson's ratio
Ngo et al. [41]	Ballast	Diameter =300mm Height =600mm	Anisotropy behaviour, mobilized friction angle

118

119

Table 2. Anisotropic tests conducted using hollow cylinder apparatus

Source	Soil type	Inner diameter/ Outer diameter/ Height (mm)	Aim
Hight et al. [14]	Sand/clay	203/254/254	Principal stress rotation effects
Tatsuoka et al. [17]	Sand	30/50/200	Anisotropy, shear strength
Pradhan et al. [18] and Pradhan et al. [19]	Sand	60/100/200	Anisotropy, shear strength
Grabe [16]	Sand	60/100/200	Principal stress rotation effects, anisotropy
Rolo [27]	Sand/clay	76/100/200	Anisotropy shear strength
Yang et al. [20]	Sand	150/314/200	Anisotropy, intermediate principal stress
Lade et al. [21] and Lade [22]	Sand	180/220/400	Principal stress rotation effects, anisotropy, Shear strength
O'Kelly and Naughton [23] and O'Kelly and Naughton [24]	Sand	71/100/200	Anisotropy, small strain, yield criterion
Yang [25] and Yang et al. [26]	Sand	60/100/200	Anisotropy, plasticity, non-coaxiality

120

121

122

Table 3. Anisotropic tests conducted using true triaxial test apparatus

Source	Soil type	Dimension of cubic sample side length (mm)	Aim
--------	-----------	--	-----

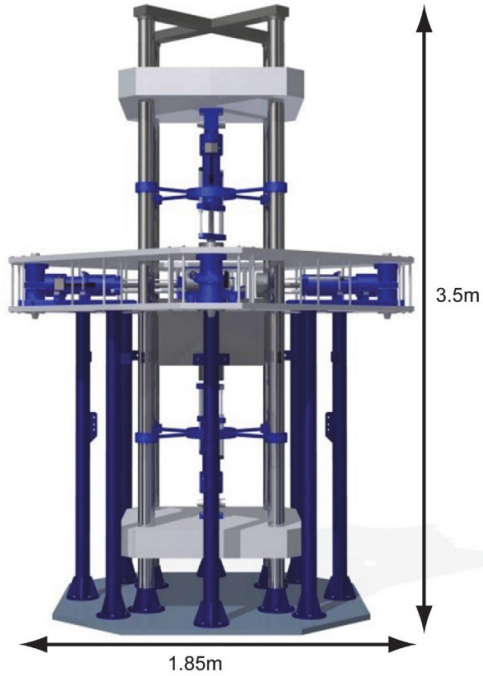
Yamada and Ishihara [30]	Sand	100mm	Anisotropy, shear strength
Sture and Desai [28] and Desai et al. [29]	Sand/ballast	101.6mm	Anisotropy, stress-strain curves
Ochiai and Lade [32]	Sand	76mm	Anisotropy, stress-strain behaviour
Reis et al. [31]	Sand	60mm	Anisotropy, saturated and unsaturated
GeoTT (present project)	Railway ballast	500mm	Anisotropy, Poisson's ratio, modulus

123

## 124 2 Apparatus development

### 125 2.1 True triaxial test rig

126 A true triaxial testing facility (hereafter called 'GeoTT') was designed for large granular  
127 particle testing in collaboration between Heriot Watt University and The University of  
128 Glasgow. It is 3.5m high and 1.85m wide, with the ability to house test samples with  
129 maximum lateral dimensions of 580mm (Figure 1). It consists of 6 independent  
130 hydraulic actuators, with 2 aligned in each Cartesian plane, making it well-suited for  
131 the large-scale testing of anisotropic behaviour (Figure 2). Also, using 6 rams instead  
132 of 3 means that a more uniform stress distribution can be applied to test samples.  
133 Thus, the effect of varying confining stress can be investigated. Each ram is connected  
134 to a load cell and a linear variable displacement transducer (LVDT) for control  
135 purposes. The control setup allows for a wide range of independent signal types to be  
136 fed into each ram.



137

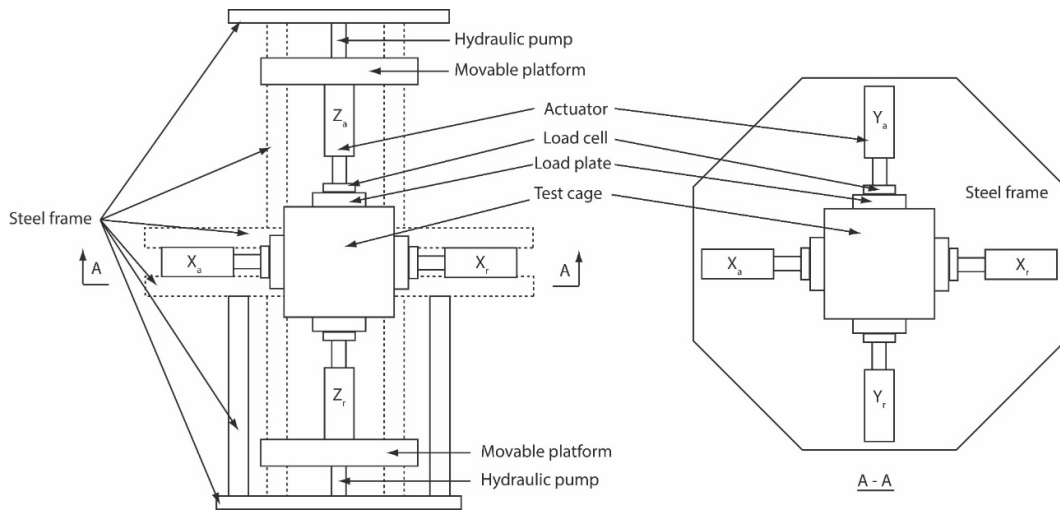
138

139

(a)

(b)

Figure 1. True triaxial testing apparatus: (a) Photograph, (b) Design drawing



140

141

142

Figure 2. Schematic of the GeoTT (Left: side view, Right Birdseye view – not to scale)

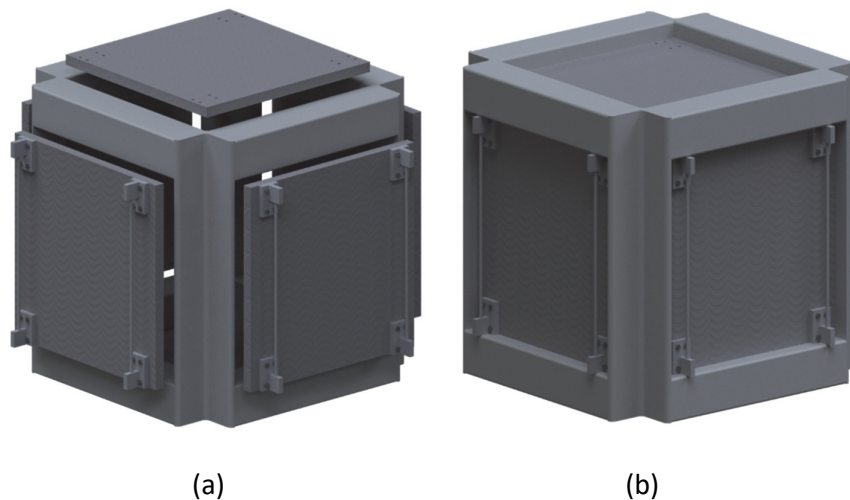
## 143 2.2 Test cage

144 A bespoke steel test cage was developed to confine the large granular particles during  
 145 testing. The outer skeleton had dimensions, 560mm x 560mm x 560mm, and 6  
 146 hollow sides. Each of these sides housed 6 separate and independently movable walls  
 147 that allowed the sample to change volume during testing (Figure 3). Each wall had a  
 148 maximum stroke of 60mm to prevent each wall colliding. The skeleton had

149 protruding protective stops (not shown) to prevent sample egress in the event of  
150 excessive wall contraction (Figure 3a). These stops were linked to the control  
151 software and the test would automatically halt if this condition was reached. Further,  
152 to prevent small granular particles from exiting the sample via the skeleton-wall  
153 clearance, the inner test cage was encased using a thin plastic membrane (see Figure  
154 4).

155 The true triaxial tests also depended upon the cage wall movement being  
156 independent from the cage skeleton. If friction was encountered at this location then  
157 the metal-on-metal contact could have introduced testing errors. During initial rig  
158 development, it was found that this friction risk was greatest in the vertical plane, due  
159 to potential sag of the horizontally orientated rams. Therefore a suspension system  
160 was developed to support the self-weight of the steel walls and load cells, thus  
161 counteracting the downward vertical force on the horizontal rams (Figure 5a). This  
162 was implemented by connecting the cage walls to the upper GeoTT frame via  
163 tuneable-length steel wires.

164 To illustrate the performance of the suspension system, Figure 5b shows a test  
165 performed during GeoTT commissioning, where the position of a lateral cage wall was  
166 cycled between the inside and outside of the cage skeleton. At the time prior to 800s  
167 (shown by the black line), the suspension system was not engaged, however, after  
168 800s it was engaged. At all data points, the measured horizontal force was recorded  
169 to quantify the potential horizontal resistance due to friction. In absence of the  
170 suspension system, the force varied from -0.20kN to 0.12kN depending upon position,  
171 while when present the force varied from -0.09kN to 0.04kN. Therefore, when the  
172 suspension system was engaged, the friction between walls and cage skeleton was  
173 significantly reduced. Accordingly, the suspension system was used for all tests  
174 presented in this paper.



175  
176  
177

Figure 3. GeoTT testing cage: (a) walls contracted, (b) walls compressed



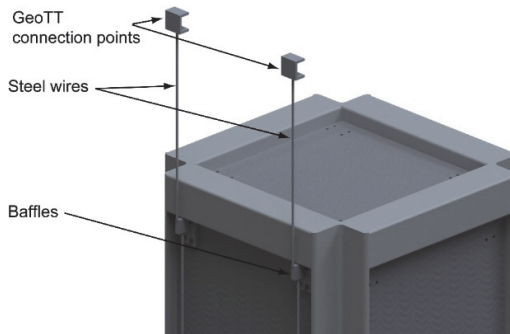


178

179

180

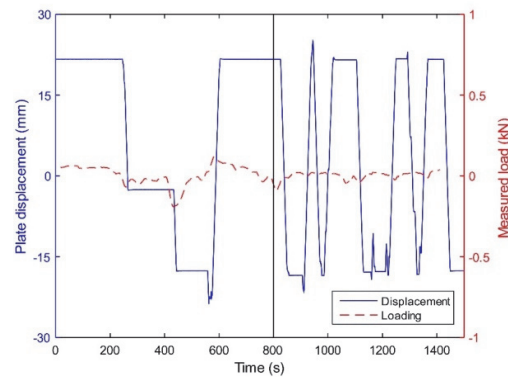
Figure 4. Inner cage with plastic sheet



181

182

(a)



(b)

183 Figure 5. Suspension system details: (a) suspension design, (b) wall-skeleton friction

### 184 3 Testing methodology

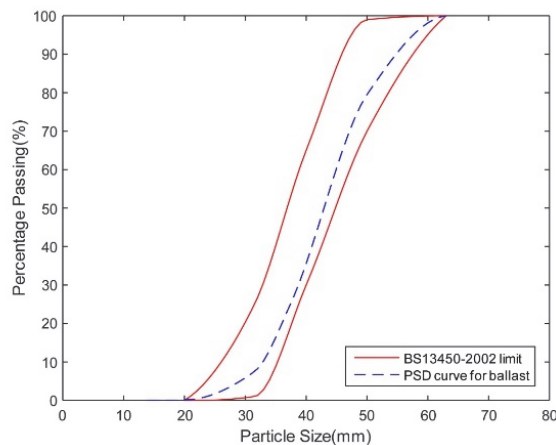
185 Two sets of tests were undertaken. First, monotonic axial loading tests were  
 186 performed for the purpose of investigating the Poisson's ratio and modulus of ballast.  
 187 Next, a combined hydrostatic loading and unloading test was performed to further  
 188 investigate the cross-anisotropic behaviour of ballast. Both tests following  
 189 independent loading plans.

#### 190 3.1 Sample preparation

191 The particle size distribution (PSD) of the railway ballast material was characterised in  
 192 accordance with BS EN 13450-2002 [42] / BS EN 13450-2013 [43], with all particles  
 193 lying in the 20-63mm range and  $d_{50} = 43\text{mm}$  (see Figure 6). The coefficient of  
 194 uniformity  $C_u$  and coefficient of curvature  $C_c$  were determined as 1.36 and 1.009  
 195 respectively, indicating the ballast was classified as uniformly graded. The ballast

196 aggregate was also washed and dried in accordance with EN 13450-2002 [42] / BS EN  
197 13450-2013 [43] and BS EN 933-1 [44]. After the ballast was prepared, it was poured  
198 into the test cage (500mm x 500mm x 500mm) in 5 stages, and each layer was  
199 compacted for exactly 10 minutes using a vibrating Kango tool to achieve a  
200 specimen density of 1,300kg/m<sup>3</sup>.

201 Although only particle size distribution tests were used to characterise the ballast, it  
202 was sourced from the same Network Rail approved quarry as the ballast used by  
203 Kwan [45]. Therefore the properties were likely to have been similar to those found in  
204 other UK ballast research works [e.g. LAA index  $\leq$  20 [46], MDE index  $\leq$  7 [47], ACV  
205  $\leq$  22% [48], Flakiness index  $\leq$  35 [49], Particle length  $\leq$  4 [50]].



206

207

*Figure 6. Ballast particle size distribution curve*

### 208 3.2 Test 1: monotonic Axial Loading

209 The six rams ( $X_a$ ,  $X_r$ ,  $Y_a$ ,  $Y_r$ ,  $Z_a$ ,  $Z_r$ ) were used to apply static compressive stresses  
210 towards ballast samples as shown in Figure 7. Subscripts 'r' and 'a' are used to  
211 differentiate between the 2 different rams in each Cartesian plane. The axial load  
212 direction was varied between the X, Y and Z planes, and had a maximum value of  
213 500kPa. Three different confining stresses (30, 60, 75kPa) were applied to the four  
214 specimen faces and each test (e.g. M1-9) was repeated three times, resulting in a  
215 total of 27 test results. The selection of these three confining stresses was based on  
216 the research from Indraratna et al. [51], where three degradation zones were  
217 identified with confining stress: less than 30kPa, 30-75kPa and larger than 75kPa. For  
218 each test, the following procedure, also summarized in Table 4, was used:

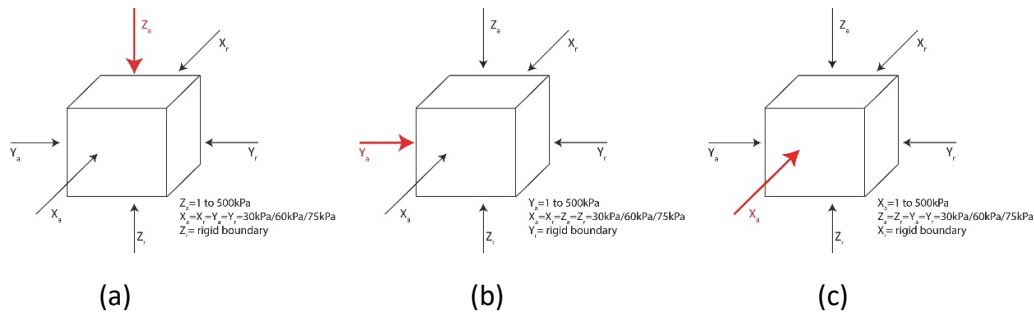
- 219
- 220 a) A constant confining stress (either 30kPa/60kPa/75kPa) was applied to the
  - 221 ballast sample in the 2 directions that were not the primary loading direction;
  - 222 b) The position of the loading plate was recorded to determine the initial length
  - 223 of the sample (L);
  - 224 c) An axial stress was applied in the primary loading direction and increased
  - 225 monotonically at a rate of 62.5kPa per minute, from an initial value of
  - 6.25kPa. The opposite ram maintained a fixed position, thus creating a rigid

- 226 boundary;
- 227 d) When the axial stress reached 500kPa, it was held constant for 5 minutes;
- 228 e) The axial stress was decreased at a rate of 62.56kPa per 10 seconds until
- 229 reaching a magnitude of 6.25kPa;
- 230 f) X, Y and Z displacements were recorded throughout steps a-e;
- 231 g) Steps a-f were repeated three times on the sample to ensure repeatability
- 232 and consistency of results;
- 233 h) Steps a-g were repeated for the remaining axial loading directions; and finally,
- 234 i) The confining stress was increased (3 values tested: 30kPa/60kPa/75kPa) and
- 235 steps a-h repeated.
- 236

237 *Table 4. Monotonic axial test procedure*

Test stage	Confining stress (kPa)	Confining direction	Axial load direction	Rigid boundary
M1	30	X and Y	Za	Zr
M2	30	X and Z	Ya	Yr
M3	30	Y and Z	Xa	Xr
M4	60	X and Y	Za	Zr
M5	60	X and Z	Ya	Yr
M6	60	Y and Z	Xa	Xr
M7	75	X and Y	Za	Zr
M8	75	X and Z	Ya	Yr
M9	75	Y and Z	Xa	Xr

238



241 Figure 7. Axial load directions: (a)  $Z_a$  loading, (b)  $Y_a$  loading, (c)  $X_a$  loading

242

### 243 3.3 Test 2: combined Hydrostatic Loading and Unloading

244 In addition to the monotonic axial loading tests, a combined hydrostatic loading and

245 unloading test was also performed to investigate the unloading response of ballast.

246 Rather than using the same procedure as for the previous monotonic tests (Table 4),

247 the hydrostatic compression test procedure outlined by Desai et al. [29] was used and

248 is summarized in Table 5:

- 249 a) A hydrostatic confining stress of 34.5kPa was applied in all 3 directions

- 250 b) The axial stress was increased in increments of 34.5kPa, from the confining  
 251 stress (34.5kPa) to 172kPa. At each increment, the deformations were  
 252 measured after they stabilized.  
 253 c) The axial stress was reduced from 172kPa to 34.5kPa in 34.5kPa increments  
 254 d) The axial stress was increased in increments of 34.5kPa, from the confining  
 255 stress (34.5kPa) to 345kPa. At each increment, the deformations were  
 256 measured after they stabilized.  
 257 e) The axial stress was reduced from 345kPa to 34.5kPa, in 34.5kPa increments  
 258 f) The axial stress was increased in increments of 34.5kPa, from the confining  
 259 stress (34.5kPa) to 517kPa. At each increment, the deformations were  
 260 measured after they stabilized.  
 261 g) The axial stress was reduced from 517kPa to 34.5kPa, in 34.5kPa increments;  
 262 h) The test was repeated for the remaining two Cartesian planes.  
 263

264

Table 5. Hydrostatic testing procedure

Test stage	Confining stress (kPa)	Deviator stress (kPa)	Confining direction	Axial load direction	Rigid boundary
H1	34.5	137.5	X and Y	Z <sub>a</sub>	Z <sub>r</sub>
H2	34.5	310.5	X and Z	Y <sub>a</sub>	Y <sub>r</sub>
H3	34.5	482.5	Y and Z	X <sub>a</sub>	X <sub>r</sub>

265

### 266 3.4 Interpretation of test results

267 When a uniaxial compressive force is applied to a cubic or cuboidal test specimen, it  
 268 contracts in the axial direction and expands in the remaining two  
 269 perpendicular/transverse directions (Figure 8). Assuming the axial stress is in the Z  
 270 direction, the resulting recoverable horizontal strains are in the X and Y directions  
 271 (see Figure 9). For this case, Equations (1), (2) and (3) give the calculation for the axial  
 272 recoverable strain in the Z direction and the horizontal (or transverse) recoverable  
 273 strains in X and Y directions, respectively. Then, the magnitude of the average  
 274 horizontal or transverse strain is calculated using Equations (4):

$$275 \quad \varepsilon_{axial} = \frac{\delta_z}{L}, \text{ (positive for axial compression)} \quad (1)$$

$$276 \quad \varepsilon_{trans_x} = \frac{\delta_x}{L}, \text{ (negative for axial compression)} \quad (2)$$

$$277 \quad \varepsilon_{trans_y} = \frac{\delta_y}{L}, \text{ (negative for axial compression)} \quad (3)$$

$$278 \quad \varepsilon_{trans} = \frac{\varepsilon_{trans_x} + \varepsilon_{trans_y}}{2} \quad (4)$$

279 Where,

280 L is the initial length of the ballast sample

281  $\delta_x$  is the recoverable displacement of ballast sample in X direction

282  $\delta_y$  is the recoverable displacement of ballast sample in Y direction

283  $\delta_z$  is the recoverable displacement of ballast sample in Z direction

284

285 Thus, Poisson’s ratio is calculated as:

286 
$$\nu = -\frac{\epsilon_{trans}}{\epsilon_{axial}} \tag{5}$$

287 and the modulus is calculated as:

288 
$$Modulus = \frac{\sigma_{axial\_time}}{\epsilon_{axial\_time}} \tag{6}$$

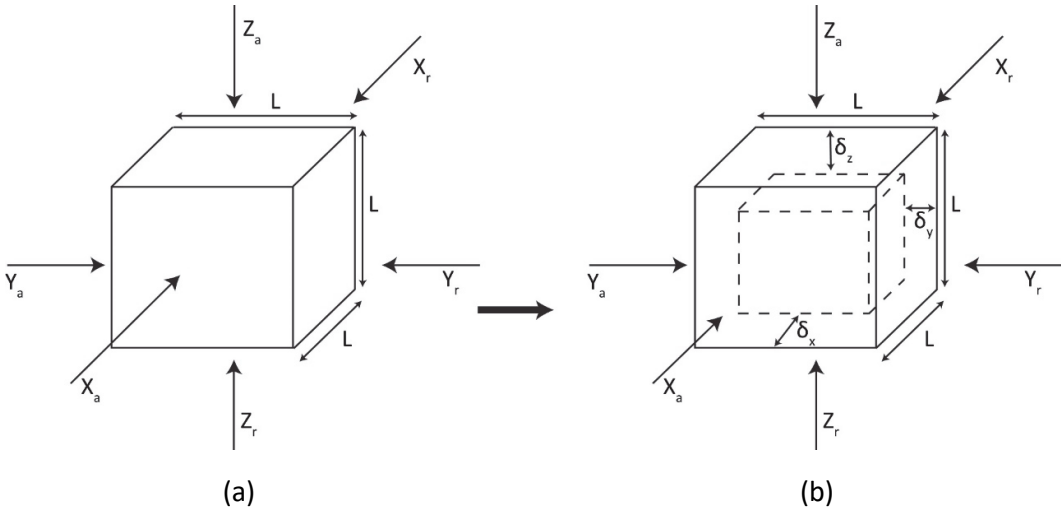
289 Where,

290  $\sigma_{axial\_time}$  is the axial stress time history

291  $\epsilon_{axial\_time}$  is the axial strain time history

292

293



294

295

296 Figure 8. Poisson’s Ratio calculation: (a) un-deformed specimen, (b) deformed  
297 specimen in dashed line

298

## 299 4 Test results and discussion

### 300 4.1 Test 1 results

#### 301 4.1.1 Poisson's ratio

302 For each confining stress and axial load pair, 3 tests were performed. As an example,  
303 Figure 9 shows the loading path and displacements in X, Y and Z directions for  
304 monotonic axial loading in the  $Z_a$  direction under a confining stress of 75kPa. The  
305 displacements were used for the calculation of strains, while only recoverable strains  
306 were used for the calculation of Poisson's ratio. It is seen that deformation did not  
307 return to zero after unloading, thus indicating plastic deformation. This plastic  
308 deformation indicated that additional sample compaction occurred in the vertical  
309 direction and additional expansion in the horizontal direction, when the primary  
310 loading was applied in  $Z_a$ .

311 Since 3 repeated tests were performed under the same confining stress and axial load  
312 direction, the mean value of Poisson's ratio was calculated to minimize the test error  
313 (e.g. the 3 Poisson' ratios in the  $Z_a$  direction from stage M1 with 30kPa confining were  
314 averaged, giving a mean Poisson's ratio of 0.31).

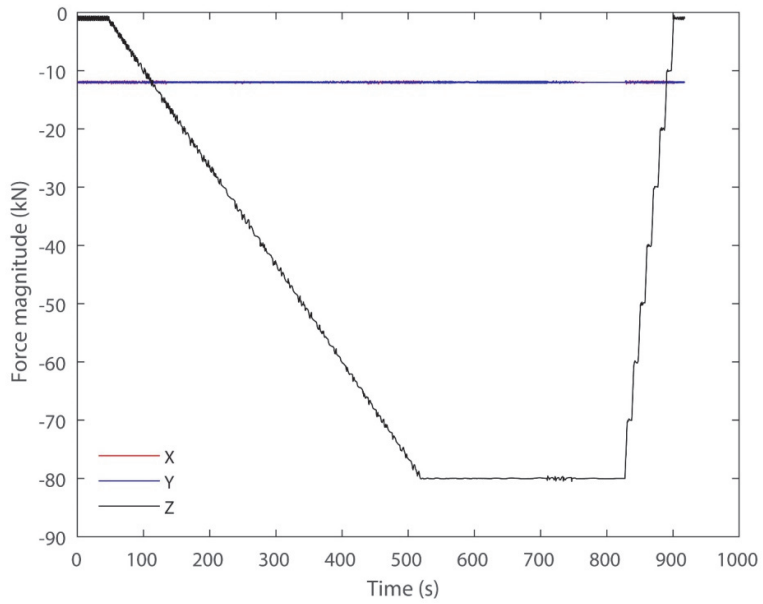
315 Figure 10 shows the relationship between confining stress and Poisson's ratio. It is  
316 seen that there was a distinct correlation, with Poisson's ratio decreasing with  
317 increased confining stress. The mean values in X, Y and Z directions were 0.28, 0.32  
318 and 0.31 at a confining stress of 30kPa. The Poisson's ratio values reduced to 0.22,  
319 0.26 and 0.23 for a confining stress of 60kPa and further reduced to 0.15, 0.19 and  
320 0.18 for a confining stress of 75kPa (Table 6). This is primarily because the increased  
321 confining stress reduced the displacement in the confining direction, resulting in a  
322 lower Poisson's ratio. This was consistent with the ballast triaxial tests performed by  
323 Indraratna et al. [52], where the initial loading stage was used for the study between  
324 confining stress and Poisson's ratio in the vertical direction. It was found that  
325 Poisson's ratio decreased with increasing confining stress. Similarly, Aursudkij et al.  
326 [40] carried out cyclic triaxial tests and found that the vertical Poisson's ratio  
327 decreased as confining stress increased from 30kPa to 60kPa under axial loading. The  
328 small discrepancies between the X and Y directions were likely because the  
329 monotonic test in the X direction was performed after the Y direction, resulting in a  
330 lower Poisson' ratio in the X direction.

331

332 Table 6. Poisson's ratios for monotonic lading in X, Y and Z directions

Confining stress (kPa)	30			60			75		
	X	Y	Z	X	Y	Z	X	Y	Z
Mean value of Poisson's ratio	0.28	0.32	0.31	0.22	0.26	0.23	0.15	0.19	0.18

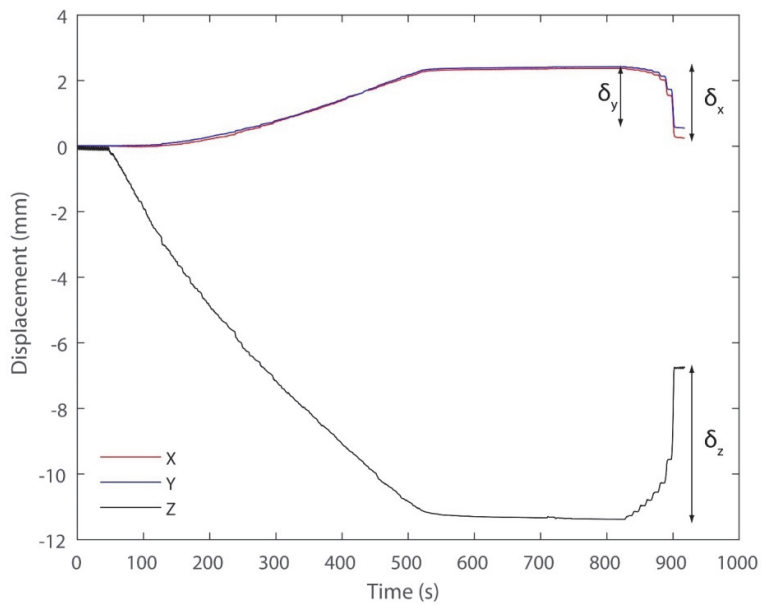
333



334

335

(a)



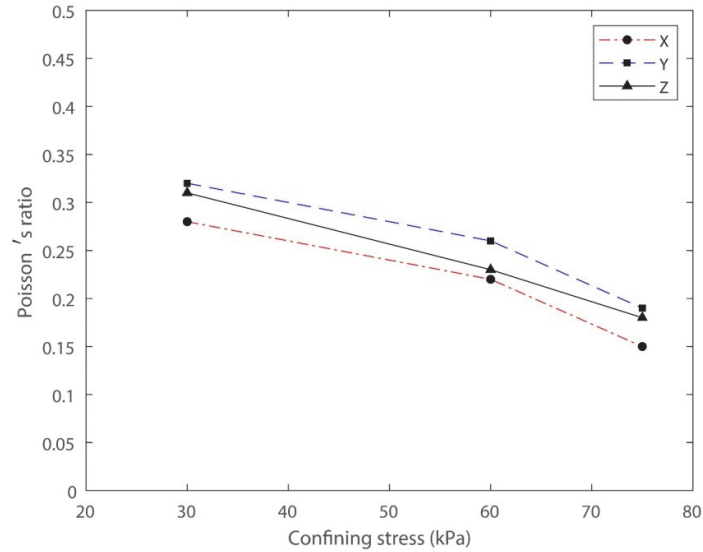
336

337

(b)

338 *Figure 9. Monotonic testing results when loading in  $Z_o$  direction under a confining*  
 339 *stress of 75kPa: (a) loading path, (b) displacements in X, Y and Z directions*

340



341

342 *Figure 10. Relationship between Poisson's ratio and axial loading direction*

343

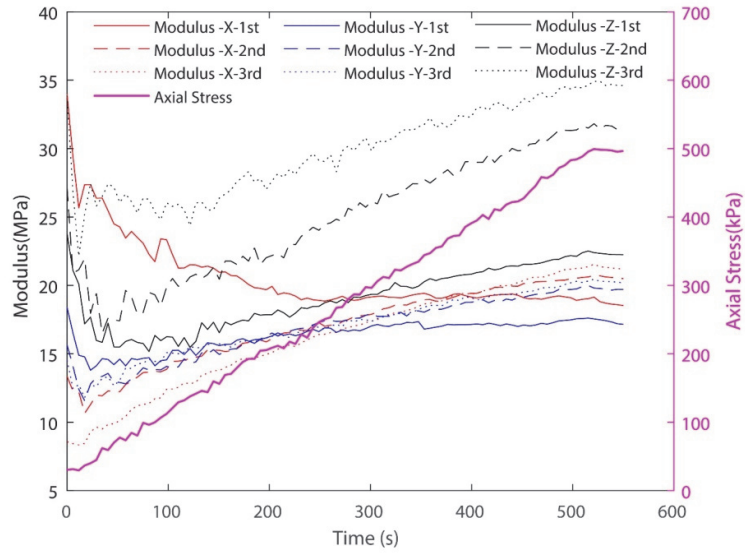
344

345 4.1.2 Modulus

346 Figure 11 shows an example of the modulus from all repeated tests in X, Y and Z axial  
 347 load directions under 75kPa confining stress. Correspondingly, Figure 12-Figure 14  
 348 show the mean modulus (average modulus across the 3 repeated tests) for confining  
 349 stresses of 30, 60 and 75kPa respectively. Considering the Z direction at 30kPa, Figure  
 350 12 shows that the modulus decreased rapidly when the axial stress was low, reached  
 351 a local minimum and then increased again steadily as axial stress was increased. This  
 352 dilation resulted in the modulus at the end of the test (500kPa) being similar to the  
 353 starting value. Regarding the X and Y directions, their responses were similar and had  
 354 modulus significantly lower than the vertical direction (Z is on average 73% higher  
 355 than X, and 66% higher than Y, when the axial stress is 500kPa). Horizontal modulus is  
 356 particularly important on railway curves where lateral forces are higher compared to  
 357 the straight track.

358 Similar findings were obtained for confining stresses of 60kPa and 75kPa. Figure 13  
 359 shows the 60kPa case where Z was on average 66% higher than X and 76% higher  
 360 than Y when the axial stress was 500kPa. Alternatively, Figure 14 shows the 75kPa  
 361 case where Z was on average 46% higher than X and 54% higher than Y when the axial  
 362 stress was 500kPa. The overall combined results are shown in Figure 15 where it can  
 363 be seen that for all directions, the lower confining stress resulted in lower modulus.  
 364 This is important for railways because different locations within the ballast layer have  
 365 different confining stress. Further, ballast layer dimensions vary across different lines,  
 366 either due to design or historical maintenance procedures. Therefore different track  
 367 sections also have different confining stresses.



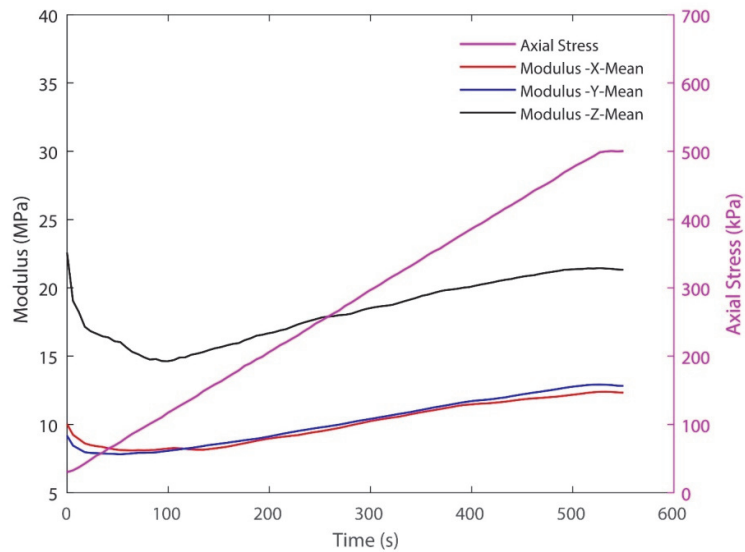


368

369 *Figure 11. Raw modulus in X, Y and Z axial load directions under 75kPa confining stress*

370

371

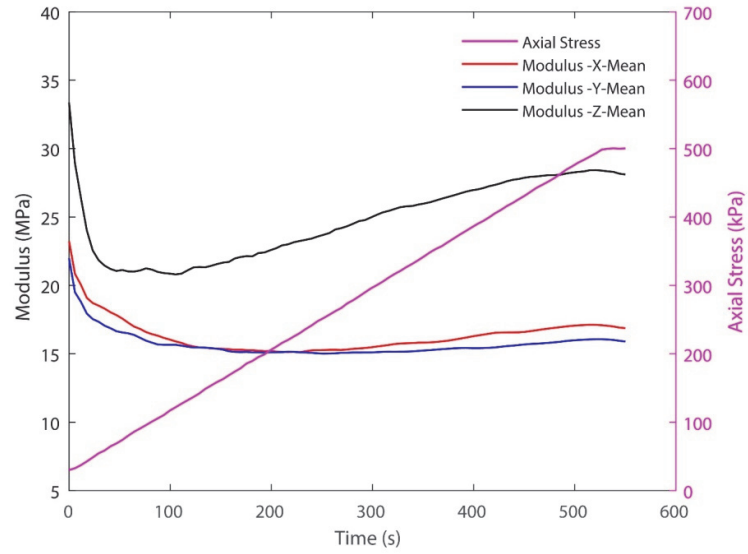


372

373 *Figure 12. Mean modulus in X, Y and Z axial load directions under 30kPa confining*  
 374 *stress*

375

376



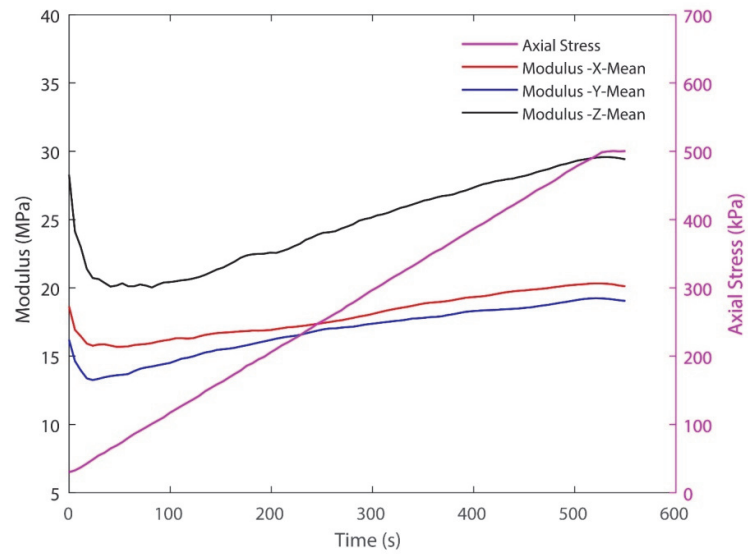
377

378

379

Figure 13. Mean modulus in X, Y and Z axial load directions under 60kPa confining stress

380



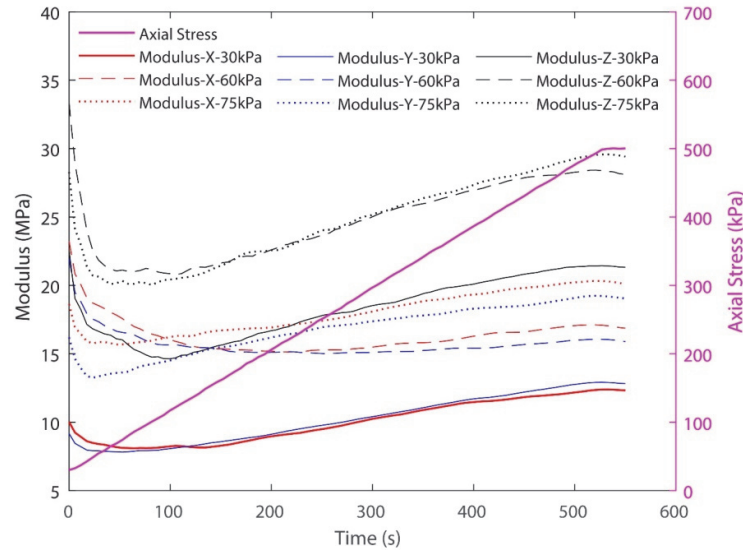
381

382

383

Figure 14. Mean modulus in X, Y and Z axial load directions under 75kPa confining stress

384



385

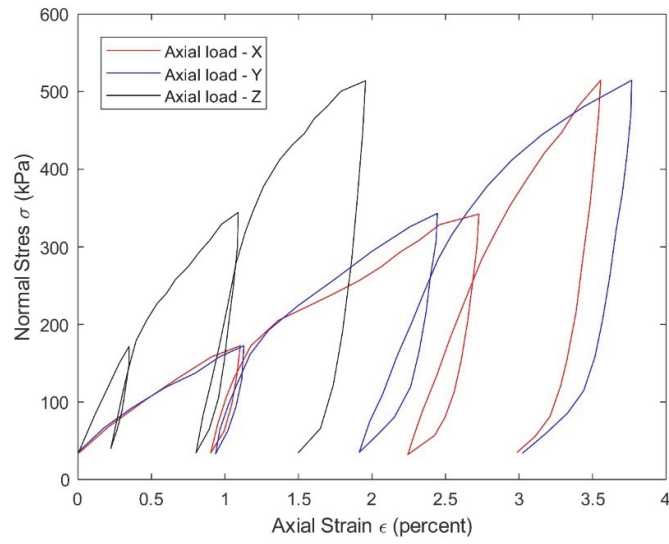
386 *Figure 15. Mean modulus in X, Y and Z axial load directions under varying confining*  
 387 *stress*

388

389 **4.2 Test 2 results**

390 Figure 16 shows the three loading and unloading cycles of the test sample.  
 391 Permanent deformation was clearly recorded after the 3 cycles in X, Y, and Z  
 392 directions, and reached maximums of 172kPa, 345kPa and 517kPa, respectively. The  
 393 horizontal directions (X and Y) exhibited approximately double the permanent  
 394 deformation (3%) compared to the vertical direction (1.5%), thus demonstrating the  
 395 typical cross-anisotropic behaviour of ballast. Based on recoverable strains after each  
 396 unloading stage, the relationship between sample modulus and deviator stress is  
 397 presented in Figure 17. It shows that sample modulus in the X and Y directions  
 398 increased from 640 MPa and 600 MPa, to 800 MPa and 700MPa respectively, when  
 399 the deviator stress was 310.5 kPa. However, the sample modulus in the Z direction  
 400 increased from 900 MPa to 1000 MPa when deviator stress reached 310.5 kPa, and  
 401 then remained constant. This change of modulus in each direction again indicated the  
 402 cross-anisotropic behaviour of the ballast sample, while this cross-anisotropic  
 403 behaviour was similar in X and Y direction in terms of unloading response and sample  
 404 modulus. However, it should be noted that the responses show discrepancies with  
 405 traditional nonlinear soil behaviour.

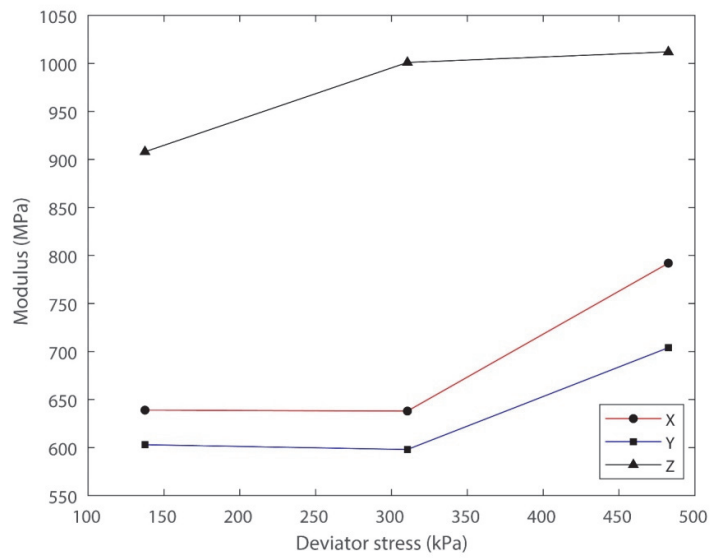
406 Upon inspection after testing, ballast breakage was noticed when removing the  
 407 sample from the test cage. Also, ballast aggregate particle cracking was heard during  
 408 testing.



409

410

Figure 16. Unloading response in all three axial load directions



411

412

Figure 17. Relationship between modulus and deviator stress

## 413 5 Conclusions

414 Railway ballast typically behaves in an anisotropic manner, with greater stiffness in  
415 the vertical compaction direction. This is important to quantify for a better  
416 understanding of the field mechanical behaviour, and for the modelling of the  
417 dynamic response behaviour. Therefore, this paper presented results for a railway  
418 ballast aggregate material tested under true-triaxial conditions. A novel, large, true-  
419 triaxial apparatus and its accompanying testing cage were successfully developed in  
420 the laboratory. The true triaxial device utilised six hydraulic actuators to ensure a  
421 uniform stress distribution across the test sample. Three confining stresses (30kPa,  
422 60kPa and 75kPa) were used to investigate Poisson's ratio, modulus and loading-  
423 unloading characteristics. Anisotropic behaviour was clearly observed for the ballast  
424 aggregate material; the horizontal response as obtained from horizontal and  
425 transverse strain measurements varied when compared to the strain values measured  
426 in the vertical direction. Both Poisson's ratio and modulus were sensitive to the  
427 applied confining stresses.

428

## 429 6 Acknowledgement

430 The authors express their gratitude to The University of Glasgow and Prof David Muir  
431 Wood for their significant efforts on the original development of the true triaxial rig.  
432 They also thank Heriot-Watt University for the support to modify the original design  
433 and adaption for ballast testing. Also, support from the University of Leeds is  
434 acknowledged along with the financial assistance from the Leverhulme Trust (PLP-  
435 2016-270).

436

437

## 438 7 References

- 439 [1] Roscoe KH, Schofield AN, Thurairajah A. Yielding of clays in states wetter than critical.  
440 *Géotechnique* 1963;13:211–40.
- 441 [2] Lade P V., Duncan JM. Elastoplastic stress-strain theory for cohesionless soil. *ASCE J*  
442 *Geotech Eng Div* 1975;101:1037–53.
- 443 [3] Van Eekelen HAM. Isotropic yield surfaces in three dimensions for use in soil  
444 mechanics. *Int J Numer Anal Methods Geomech* 1980;4:89–101.
- 445 [4] Sagaseta C. Analysis of undrained soil deformation due to ground loss. *Géotechnique*  
446 1987;37:301–20.
- 447 [5] Alonso E., Gens A, Josa A. A constitutive model for partially saturated soils.  
448 *Géotechnique* 1990;40:405–30.
- 449 [6] Laloui L, Cekerevac C. Thermo-Plasticity of Clays: An Isotropic Yield Mechanism.  
450 *Comput Geotech* 2003;30:649–660.
- 451 [7] Rotta G V., Consoli NC, Prietto PDM, Coop MR, Graham J. Isotropic yielding in an  
452 artificially cemented soil cured under stress. *Géotechnique* 2003;53:493–501.
- 453 [8] Alonso EE, Pinyol NM, Gens A. Compacted soil behaviour: initial state, structure and  
454 constitutive modelling. *Géotechnique*, 2012;V1:134p.
- 455 [9] Miura, Seiichi and Toki S. Anisotropy in mechanical properties and its simulation of  
456 sands sampled from natural deposits. *Soils Found* 1984;24:69–84.
- 457 [10] Tutumluer E. Predicting behavior of flexible pavements with granular bases. PhD  
458 Thesis, Georgia Institute of Technology, 1995.
- 459 [11] Tutumluer E, Thompson MR. Anisotropic modeling of granular bases in flexible  
460 pavements. *J Transp Res Board* 1997;TRR 1577:18–26.
- 461 [12] Tutumluer E, Kwon J. Validations of Anisotropic Aggregate Base Behavior from Full-  
462 Scale Pavement Tests. *Contemp Top Gr Modif Probl Soils, Geo-Support*, Reston, VA:  
463 American Society of Civil Engineers; 2009, p. 441–8.
- 464 [13] Cooling LF, Smith DB. The Shearing Resistance of Soils. *J Inst Civ Eng* 1936;3:333–43.
- 465 [14] Hight DW, Gens A, Symes MJ. The development of a new hollow cylinder apparatus for  
466 investigating the effects of principal stress rotation in soils. *Géotechnique*  
467 1983;33:355–83.
- 468 [15] Saada A. State-of-the-Art Paper: Hollow Cylinder Torsional Devices: Their Advantages  
469 and Limitations. *Adv Triaxial Test Soil Rock*, 100 Barr Harbor Drive, PO Box C700, West  
470 Conshohocken, PA 19428-2959: ASTM International; 1988, p. 766-766–24.
- 471 [16] Grabe PJ. Resilient and permanent deformation of railway foundations under principal  
472 stress rotation. PhD Thesis, University of Southampton, 2003.
- 473 [17] Tatsuoka F, Sonoda S, Hara K, Fukushima S, Pradhan TBS. Failure and deformation of  
474 sand in torsional shear. *Soils Found* 1986;26:79–97.
- 475 [18] Pradhan, T.B.S., Tatsuoka, F. and Horii N. Simple shear testing on sand in a torsional  
476 shear apparatus. *Soils Found Japanese Soc Soil Mech Found Eng* 1988;28:95–112.
- 477 [19] Pradhan, T.B.S., Tatsuoka, F. and Horii N. Strength and deformation characteristics of

- 478 sand in torsional simple shear. *Soils Found* 1988;28:131–48.
- 479 [20] Yang ZX, Li XS, Yang J. Undrained anisotropy and rotational shear in granular soil.  
480 *Géotechnique* 2007;57:371–84.
- 481 [21] Lade P V., Nam J, Hong WP. Shear banding and cross-anisotropic behavior observed in  
482 laboratory sand tests with stress rotation. *Can Geotech J* 2008;45:74–84.
- 483 [22] Lade P V. Failure Criterion for Cross-Anisotropic Soils. *J Geotech Geoenvironmental*  
484 *Eng* 2008;134:117–24.
- 485 [23] O’Kelly BC, Naughton PJ. Development of a new hollow cylinder apparatus for stress  
486 path measurements over a wide strain range. *Geotech Test J* 2005;28:345–54.
- 487 [24] O’Kelly BC, Naughton PJ. Study of the yielding of sand under generalized stress  
488 conditions using a versatile hollow cylinder torsional apparatus. *Mech Mater*  
489 2009;41:187–98.
- 490 [25] Yang L. Experimental study of soil anisotropy using hollow cylinder testing. PhD Thesis,  
491 University of Nottingham, 2013.
- 492 [26] Yang LT, Li X, Yu HS, Wanatowski D. A laboratory study of anisotropic geomaterials  
493 incorporating recent micromechanical understanding. *Acta Geotech* 2016;11:1111–29.
- 494 [27] Rolo R. The anisotropic stress-strain-strength behaviour of brittle sediments. PhD  
495 Thesis, Imperial College London (University of London), 2004.
- 496 [28] Sture S, Desai CS. Fluid cushion truly triaxial or multiaxial testing device. *Geotech Test J*  
497 1979;2:20–33.
- 498 [29] Desai CS, Siriwardane HJ, Janardhanam R. Interaction and load transfer through track  
499 support systems, Parts 2. Final Rep, DOT/RSPA/DMA-50/83/12, Off Univ Res Dept  
500 Transp Washington, DC 1983.
- 501 [30] Yamada Y, Ishihara K. Anisotropic deformation characteristics of sand under three  
502 dimensional stress conditions. *Japanese Soc Soil Mech Found Eng* 1979;19:79–94.
- 503 [31] Reis RM, de Azevedo RF, Botelho B, Severino N, Vilar OM. Performance of a cubical  
504 triaxial apparatus for testing saturated and unsaturated soils. *Geotech Test J*  
505 2011;34:1.
- 506 [32] Ochiai H, Lade PV. Three-Dimensional Behavior of Sand with Anisotropic Fabric. *J*  
507 *Geotech Eng* 1983;109:1313–28.
- 508 [33] Abelev A V, Lade P V. Effects of cross anisotropy on three-dimensional behavior of  
509 sand. I: Stress-strain behavior and shear banding. *J Eng Mech* 2003;29:160–6.
- 510 [34] Abelev A V., Lade P V. Characterization of Failure in Cross-Anisotropic Soils. *J Eng Mech*  
511 2004;130:599–606.
- 512 [35] Tutumluer E, Seyhan U. Laboratory Determination of Anisotropic Aggregate Resilient  
513 Moduli Using an Innovative Test Device. *Transp Res Rec J Transp Res Board*  
514 1999;1687:13–21.
- 515 [36] Seyhan U, Tutumluer E. Anisotropic Modular Ratios as Unbound Aggregate  
516 Performance Indicators. *J Mater Civ Eng* 2002;14:409–16.
- 517 [37] Nitchiporovitch AA. Shearing strength of coarse shell materials. *Proc 7th Int Conf Soil*  
518 *Mech Found Eng Mex*, 1969, p. 211–6.

- 519 [38] Fagnoul A, Bonnechere F. Shear strength of porphyry materials. Proc 7th Int Conf Soil  
520 Mech Found Eng Mex, 1969, p. 61–5.
- 521 [39] Marachi ND, Chan CK, Seed HB. Evaluation of properties of rockfill materials. J Soil  
522 Mech Found Div 1972;97.
- 523 [40] Aursudkij B, McDowell GR, Collop AC. Cyclic loading of railway ballast under triaxial  
524 conditions and in a railway test facility. Granul Matter 2009;11:391–401.
- 525 [41] Ngo NT, Indraratna B, Rujikiatkamjorn C. Micromechanics-Based Investigation of  
526 Fouled Ballast Using Large-Scale Triaxial Tests and Discrete Element Modeling. J  
527 Geotech Geoenvironmental Eng 2017;143:04016089.
- 528 [42] BSI. BS EN 13450 Aggregates for railway ballast. Br Stand Inst 2002.
- 529 [43] BSI. BS EN 13450 Aggregates for railway ballast. Br Stand Inst 2013.
- 530 [44] BSI. BS EN 933-1. Tests for geometrical properties of aggregates Part 1: Determination  
531 of Particle Size Distribution - Sieving Method. Br Stand Inst 2005;3:1–7.
- 532 [45] Kwan C. Geogrid Reinforcement of Railway Ballast. PhD Thesis, University of  
533 Nottingham, 2006.
- 534 [46] BSI. BS EN 1097-2. Tests for mechanical and physical properties of aggregates.  
535 Methods for the determination of resistance to fragmentation. Br Stand Inst 2010.
- 536 [47] BSI. BS EN 1097-1. Tests for mechanical and physical properties of aggregates.  
537 Determination of the resistance to wear (micro-Deval). Br Stand Inst 2011.
- 538 [48] BSI. BS 812-111. Testing aggregates. Methods for determination of ten per cent fines  
539 value (TFV). Br Stand Inst 1990.
- 540 [49] BSI. BS EN 933-3. Tests for geometrical properties of aggregates. Determination of  
541 particle shape. Flakiness index. Br Stand Inst 2012.
- 542 [50] BSI. BS EN 933-2. Tests for geometrical properties of aggregates. Determination of  
543 particle size distribution. Test sieves, nominal size of apertures. Br Stand Inst 1996.
- 544 [51] Indraratna B, Nimbalkar S, Christie D. The Performance of Rail Track Incorporating the  
545 Effects Of Ballast Breakage, Confining Pressure and Geosynthetic Reinforcement. Bear  
546 Capacit Roads, Railw Airfields 8th Int Conf, 2009.
- 547 [52] Indraratna B, Ionescu D, Christie HD. Shear behavior of railway ballast based on large-  
548 scale triaxial tests. J Geotech Geoenvironmental Eng 1998;124:439–49.
- 549